AIAA 96-2187

Rayleigh Scattering Measurements in Supersonic Facilities

B. Shirinzadeh, R. Jeffrey Balla, and M. E. Hillard
NASA Langley
Hampton, VA

19th AIAA Advanced Measurement and Ground Testing Technology Conference
June 17-20, 1996 / New Orleans, LA

Rayleigh Scattering Measurements in Supersonic Facilities

B. Shirinzadeh*, R. Jeffrey Balla*, and M. E. Hillard*
NASA Langley Research Center
Hampton, VA 23681

Abstract--Using a narrow-band, pulsed, ArF excimer laser and a single-intensified CCD camera, planar laser Rayleigh scattering measurements were performed to obtain quantitative density measurements both in the free stream and in a model flow field. These measurements were conducted in the 15-inch, Mach 6 high temperature facility at NASA Langley Research Center. This facility is capable of achieving stagnation temperatures up to 700 K (800 °F) over a range of stagnation pressures from 0.35 to 2.07 MPa (50 to 300 psia). The high temperature capability of this facility eliminates the clustering effect observed in earlier Mach 6 studies, and allows quantitative density measurements in the free stream over a range of stagnation pressures from 0.35 to 1.75 MPa (50 to 250 psia). Model flow field measurements were obtained on 38.1 mm diameter cylinder. Measurement locations include the free stream, the region behind the bow shock in front of the model, and the region behind the model including the wake. The densities deduced from the Rayleigh scattering measurements in the model flow field are compared with CFD computations. Measurement uncertainties and the detection limit are discussed.

INTRODUCTION

Quantitative, non-intrusive measurements of flow parameters such as density, temperature, and velocity play an important role in fluid mechanics. In recent years, the possibility of using the Rayleigh scattering technique to obtain quantitative flow density measurements in hypersonic facilities has been investigated.[1-3] Results of those measurements indicate that clusters are formed as a result of the cooling that takes place during the expansion process. The Rayleigh scattered signal due to the clusters was observed to be much larger than the molecular signal level with a strong dependence on the stagnation conditions, namely, the pressure and the temperature. It was also found that, for a given stagnation pressure, as the stagnation temperature was increased, the Rayleigh signal approached the molecular signal levels in the free stream of a Mach 6 facility. For this reason, the present tests were conducted at the Mach 6, high temperature facility at NASA Langley Research Center.[4] The purpose of these studies was first to obtain a range of stagnation conditions for which molecular Rayleigh signal levels can be obtained in the free stream of this facility, and second to obtain quantitative density measurements on a simple model (a cylinder) and compare the results with the CFD calculations. In doing so, the experimental difficulties associated with the facility implementation of this technique were also investigated. In this paper, quantitative density measurements obtained using the Rayleigh scattering technique, both in front and behind a cylindrical model, are presented. Measurement uncertainties both random and systematic are discussed. A comparison between the Rayleigh results and the CFD computation[5] will indicate that, within the uncertainties of the measurements and the limitations of the CFD model (spatial resolution and laminar boundary layer), an agreement between the two has been obtained. It will be also shown that with further improvements in the experimental apparatus and the facility conditions, this technique can be used to obtain quantitative density measurements in Mach 6 flows with reduced uncertainty and, perhaps, on a routine basis.

EXPERIMENTAL

Fig. 1 shows a schematic diagram of the experiment. As before,[3] a narrow-band pulsed ArF excimer laser was used as the light source. This output near 193 nm was formed into a sheet by using a 2.29 m focal length cylindrical lens (CL). The sheet measured 8.5 mm in height and about 0.5 mm in width at the focal region. The laser beam entered the facility from the top through a wedged window and a series of apertures.

* Optical Physicist, Measurement Science and Technology Branch, Research and Technology Group.

After traversing the flow field the laser beam was dumped inside the facility. The Rayleigh scattered light was collected by two lenses and was imaged onto a single-intensified charge-coupled device (CCD) camera. The signal from the camera was first processed by a distribution amplifier whose outputs went to a monitor and a time-code generator. The outputs from the time-code generator were processed by a video tape recorder and a frame grabber (digitizer). The time-code generator added a time code to the signal making it possible to correlate the video tape recorder to the digitized frame grabber signal. The signal from the frame-grabber was stored in the computer for further analysis.

To minimize uncertainties associated with the laser intensity fluctuations (spatial and temporal), a small portion of the laser beam was split off from the main beam, was attenuated to avoid detector saturation and was detected using a linear photodiode array. The linear photodiode array consisted of 1024 pixels. Each pixel measured 0.025 mm in width and 2.5 mm in height. The array was placed at the focus of the cylindrical lens. The diode array was scanned twice for each laser pulse. The scanning sequence was as follows: line reset immediately before the laser fire (charged up all photodiodes), laser fire, scan the diodes, line reset, and scan the diodes again to account for the background in the absence of the laser. These scans were digitized and stored in the computer separately. The difference between these two scans represent the signal due to the laser only. The diode array and the digitizer were externally clocked (scanned) at a rate of 50 KHz/pixel. Clock pulses for the digitizer were appropriately delayed from the clock pulses for the diode array to insure correct reading. Care was taken to insure that the scanning rate was fast enough to reduce the dark count, yet slow enough to insure that the pixels on the diode array would acquire the full charge after each scan. In addition to the diode array, for every laser shot, the total laser intensity was also monitored by another photodiode (PD) and sample-and-hold detection system. The signal from sample-and-hold detection system was digitized and stored in the computer separately. This was done as a double check of the linearity of the diode array. Proper operation is insured by comparing the normalized sum of all the pixels in the array to the signal from the photodiode/sample-and-hold detection system for each shot. It also helped to monitor the laser intensity during the run, since an analysis of the diode array signal during the run was not possible.

For these experiments the ArF excimer laser was operated at a repetition rate of 10 Hz. The laser pulse duration was about 15 nsec which allowed snapshots of the frozen flow to be obtained. The laser was operated in the narrow-band mode (seeder/oscillator) with an output energy of 120 mJ/pulse. The wavelength of the laser was tuned between O_2 transitions in the 4-0 band near the peak of the laser gain profile to minimize the absorption of the laser beam as it travelled through room air. This experimental arrangement was designed to minimize the distance between the laser and the test section along with the number of mirrors required to direct the beam into the facility.

The planar Rayleigh scattering data were collected by a two-element refractive lens and were imaged onto a gated (gate width = 0.09 msec), single-intensified CCD camera. To determine the magnification of the lens and spatial resolution of the lens/camera system, an aluminum grid was placed in the test section at the location of the laser beam. The grid was illuminated by the scattered laser light from a rough surface and an image of the grid was recorded by the camera. In this way, the magnification of the lens was determined to be 4.3 for this imaging configuration. This resulted in pixel resolutions of 0.13 mm along the direction of the laser and 0.16 mm perpendicular to the laser beam in the test section. The actual spatial resolution of the combination of the lens/camera system in the test section was determined to be 0.4 mm and 0.5 mm along and perpendicular to the laser beam direction, respectively.

The spatial correlation between the camera and the diode array was obtained by placing a line grid (G) in the laser beam (Fig. 1). The grid blocked the laser beam at various locations. Images of this laser pattern were obtained and averaged for both the camera and the diode array. For a given camera pixel-row perpendicular to the laser beam, the location of the maximum and the minimum intensities were determined and correlated to the diode array maximum and minimum intensity locations. This was done for every camera pixel-row perpendicular to the laser beam direction. From this spatial correlation, a mapping between the camera and the diode array pixels was obtained. Since the diode array had a higher resolution than the camera (~6.5 diode array pixels correspond to one camera pixel) it was possible to normalize each camera pixel to a corresponding diode array pixel determined from this mapping. An important issue in this normalization procedure was the difference in the spatial frequency response between the two detectors. To account for this difference a 23-point (0.575 mm) running average was performed on the diode array signal before the

camera signal was normalized to it. With this normalization per shot, under the laboratory conditions, it was possible to reduce the noise by almost a factor of 2 compared to that with no normalization. It also helped to obtain a better calibration, since it was noted that during the calibration procedure, the laser profile shifted in intensity.

As before,[2] it was necessary to calibrate the laser/camera system in order to obtain quantitative density measurements. This calibration was performed by pumping the tunnel down and obtaining the Rayleigh data as a function of the static pressure in the facility (no supersonic flow). Since the particle loading in this facility was higher than expected, the facility was purged during this calibration procedure with a slow flow of dry air while keeping the pressure constant through continuous pumping. For each calibration point and tunnel run, 45 images were obtained and normalized to the laser intensity profile on a per shot basis. Those frames with particles present (typically several frames per calibration set point) were omitted from the calibration. The remaining normalized images were then averaged and a linear plot of the Rayleigh signal as a function of the pressure was obtained for each pixel in the camera. From these linear plots, the slope and the intercept with their corresponding uncertainties were determined for each camera pixel and were stored in the computer. These data were used later to convert the Rayleigh signal levels obtained during the tunnel runs to molecular density.

The facility used for these experiments was the 15-inch, Mach 6 High Temperature facility at NASA Langley Research Center.[4] This facility is capable of achieving stagnation temperatures up to 700 K (800 ^{o}F) over a range of stagnation pressures from 0.35 to 2.07 MPa (50 to 300 psia). The model used for these experiments was an aluminum cylindrical model with a 38.1 mm diameter and a length of 15.24 cm. The model was equipped with pressure taps which were located around the center line. The origin of the coordinate system for these experiments was located at the center of the model. The x-direction is taken to be along the direction of the flow, the y-direction is from the bottom to the top of the facility which is opposite to the laser beam direction, and the z-direction is taken to be along the cylinder axis toward the observation window. The laser beam was fixed at a distance of z = 4 cm for all the experiments; this makes the relationship of the laser beam and the camera fixed. Various flow regions were investigated by moving the model in the x and y direction with respect to the laser beam.

Results and Discussion

Fig. 2 shows planes of the deduced densities obtained from the Rayleigh scattering measurements that were performed both in front and behind the 38.1 mm diameter cylindrical model. For the sake of comparison here, the computed densities obtained from the CFD are also plotted in this figure. For presentation purposes, 5 equally spaced gray levels are used in this figure,i. e., the bright and dark regions only represent the division marks for the gray scales used and not the high and low density regions. For these data, the facility was operated at the stagnation pressure of 1.38 MPa (200 psia) and a stagnation temperature of 672 K (750 ^{o}F) with a free stream Mach number of 6.032. To obtain each plane of the Rayleigh data, the laser/camera system was fixed and the model was moved to the desired location.

Due to the model movement during the run, an accurate measurement of the location of the laser beam with respect to the model was not possible in these experiments. The positions of the planes of the Rayleigh data with respect to the model were based on the knowledge of injection height from the center line (y axis), and the beam location from the surface of the model before and after the run (x axis). For positions of the laser beam near the surface of the model, sometimes the x-position was determined from the small scattering of the laser beam from the surface of the model. An estimate of the uncertainty in these positions is $\pm$ 1 mm. Within this uncertainty, the y-positions were adjusted based on the symmetry argument (planes (I) and (III)) or the shock shape (plane (II)). The only adjustment to the x-position was made on plane (I), which was based on the shock standoff from the model. Each plane of data here represents an average of 45 Rayleigh images which have been normalized to the laser intensity profile on a per shot basis. The averaged image obtained in this way has been processed by the calibration procedure where the observed signal levels are converted to density. A detailed comparison between the Rayleigh and the CFD data will be presented along the profiles "A", "B", and "C" shown in this figure.

Fig. 3 shows a comparison between the CFD and the Rayleigh data as a function of position along the profile "A" (y/D = 0) as is depicted in Fig. 2. Here the coordinates are non-dimensionalized by the cylinder diameter, D = 38.1 mm. The solid line in the Rayleigh data represents the average density (non-dimensionalized by the free stream density) and the dashed lines represent the statistical uncertainty (1 sigma) of the mean value of these data. This uncertainty includes the density fluctuations, the laser

intensity fluctuations, the camera noise, the shot noise, and the uncertainty associated with the calibration; but, it does not include any systematic uncertainty. For example, sometimes a movement ($\leq$ 1 camera pixel) was detected between the camera and the diode array. This movement was observed only after a tunnel run and was most likely due to an increase in the environmental temperature as a result of a tunnel run (thermal expansion in the optical rails). Although attempts were made to detect and correct the data for this shift, this systematic error can not completely be removed without going through a whole calibration procedure again. This is because of the mismatch that exists in the spatial frequency response between the camera and the diode array. The calibration procedure accounts for most of this mismatch. In Fig. 3, it is seen that agreement within the statistical uncertainty of the measurement has been obtained between the CFD and the Rayleigh data for the region behind the shock. The overall variation (systematic) in the Rayleigh data in this region is most likely due to the argument given above. For the shock region, the Rayleigh data exhibits a better spatial resolution than the CFD calculations. The spatial resolution of the CFD results decreases rapidly (larger grid points) as the distance from the model surface is increased. This explains why the Rayleigh and the CFD results do not agree for the region across the shock; however, they do agree in the free stream far from the model.

Fig. 4 shows a comparison between the Rayleigh and the CFD results along the profile "B" in Fig. 2 at two x/D locations of -0.66 and -0.70. Again, the solid line is the averaged Rayleigh data and the dashed lines are the statistical uncertainty in these data. It is noted that the CFD and the Rayleigh results agree within the uncertainty of the measurements for the region behind the shock in both profiles. Furthermore, there is no systematic variation, such as those discussed for Fig. 3, in the Rayleigh data here; since these data represent densities along the direction of the laser beam. From this plot it is also seen that the signal-to-noise in the Rayleigh data degrades along the x-axis as the edges of the laser beam are approached. The variation in the spatial resolution of the CFD as a function of the distance from the model is also apparent when examining the CFD data through the shock for the two x/D positions. It is also observed that the Rayleigh data obtained in the free stream for the two x/D positions agree within the uncertainty of the measurements.

Finally, Fig. 5 shows a plot of the Rayleigh and the CFD data along the profile "C" in Fig. 2. This profile passes through two planes of data, namely, (II) and (III). The data in plane II were corrected for a shift ($<$ 1 camera pixel) between the diode array and the camera. This correction only effects the data along the x-axis (see the discussion for Fig. 3). Also, since the signal in plane III is decreasing rapidly along the y-axis, this data becomes more susceptible to the background light scattered in the facility. An investigation of the data obtained during the calibration and the run indicated that the signal outside the laser beam (background) stayed the same for all the calibration data points, yet was increased during the facility run. The data in plane III was therefore corrected for this difference in background by subtracting a constant value from the averaged image before the Rayleigh signals were converted to density. This was the only correction performed on the data in plane III of Fig. 2. Again, the averaged deduced densities are plotted in Fig. 5 as the solid line with their corresponding statistical uncertainty as the dashed lines. The statistical uncertainty here is smaller than those presented in the previous plots. This is due to a better calibration that was obtained for this location. In Fig. 5, the split in the data due to the two measurement planes is also apparent at y/D = 1. This mismatch between the two data sets is an indication of the reproducibility of the measurements. In general, the Rayleigh and the CFD agree for the region behind the shock up to the wake region, where the Rayleigh results show a smaller wake than the CFD. The CFD calculations were performed for the laminar boundary layer which may not accurately describe this experiment; since the separation point depends on the nature of the boundary layer. The discrepancy between the CFD and the Rayleigh data in the region $-1 < y/D < 1$ may be explained by a non-constant background. For the region near the shock, the CFD exhibits a poor spatial resolution compared to the Rayleigh data. Finally, the Rayleigh data accurately predicts the free stream densities.

CONCLUSIONS

In this paper, the capability of the Rayleigh scattering technique for quantitative density measurements in a Mach 6 flow has been demonstrated. Results indicate that the densities deduced from the Rayleigh measurements performed on a cylindrical model are in agreement with the CFD calculations within the uncertainty of the measurements and the limitations of the CFD. Based on the discussions presented here, further improvements in the accuracy of the measurement

may be possible through an increase in the signal-to-noise ratio and removal of the systematic errors.

ACKNOWLEDGEMENTS

The authors are grateful to Charles Miller for providing the facility time and support to conduct these experiments. We would also thank Duane Melson and Mark Sanetrik, who kindly provided us with the CFD results presented here. Expert electronic design by Ray Gregory and mechanical design by Bruce Barnes is also acknowledged.

REFERENCES

1. B. Shirinzadeh, M. E. Hillard, and R. J. Exton, "Condensation Effects on Rayleigh Scattering Measurements in a Supersonic Wind Tunnel," AIAA Journal, vol. 29, pp. 242-246, Feb. 1991.
2. B. Shirinzadeh, M. E. Hillard, A. B. Blair, and R. J. Exton, "Study of Cluster Formation and its Effects on Rayleigh and Raman Scattering Measurements in a Mach 6 Wind Tunnel," AIAA paper 91-1496, June 24-26, 1991.
3. B. Shirinzadeh, M. E. Hillard, R. J. Balla, I. A. Waitz, J. B. Anders, and R. J. Exton, "Planar Rayleigh Scattering Results in Helium-air Mixing Experiments in a Mach-6 Wind Tunnel," Appl. Opt., vol. 31, pp. 6529-6534, Oct. 1992.
4. J. S. Hodge, "The Langley 15-inch Mach 6 High Temperature Tunnel," AIAA paper 92-3938, July 6-8, 1992.
5. D. N. Melson and M. D. Sanetrik, Computational Aerodynamics Branch, NASA Langley Research Center, private communication.

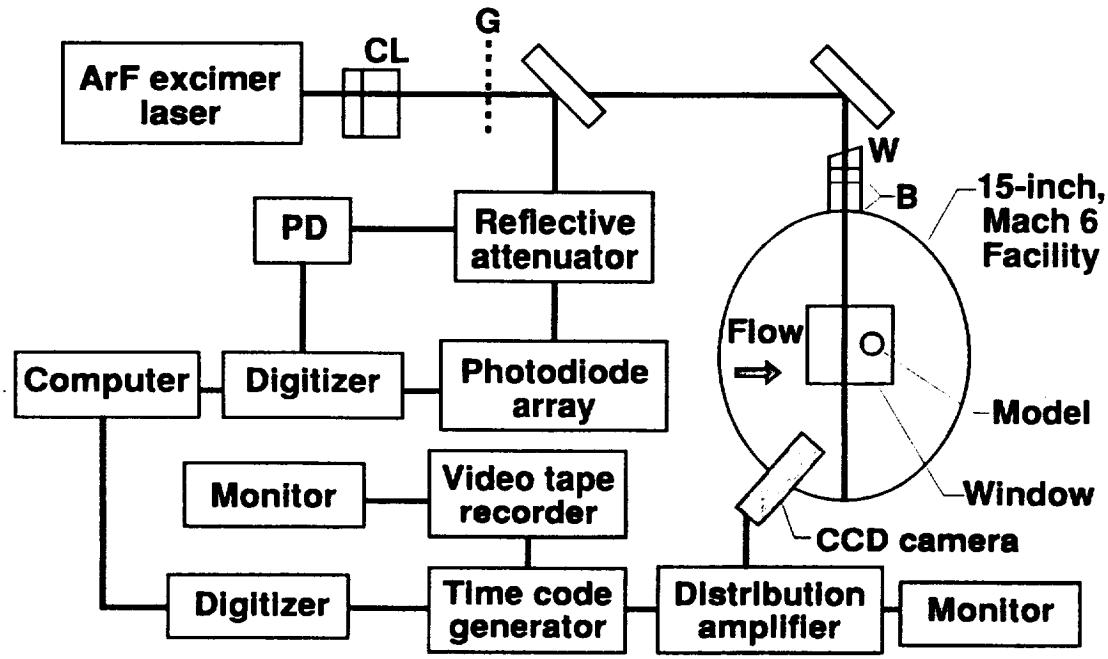

Fig. 1. Schematic diagram of the experimental setup in the 15-inch, Mach 6 high temperature tunnel.

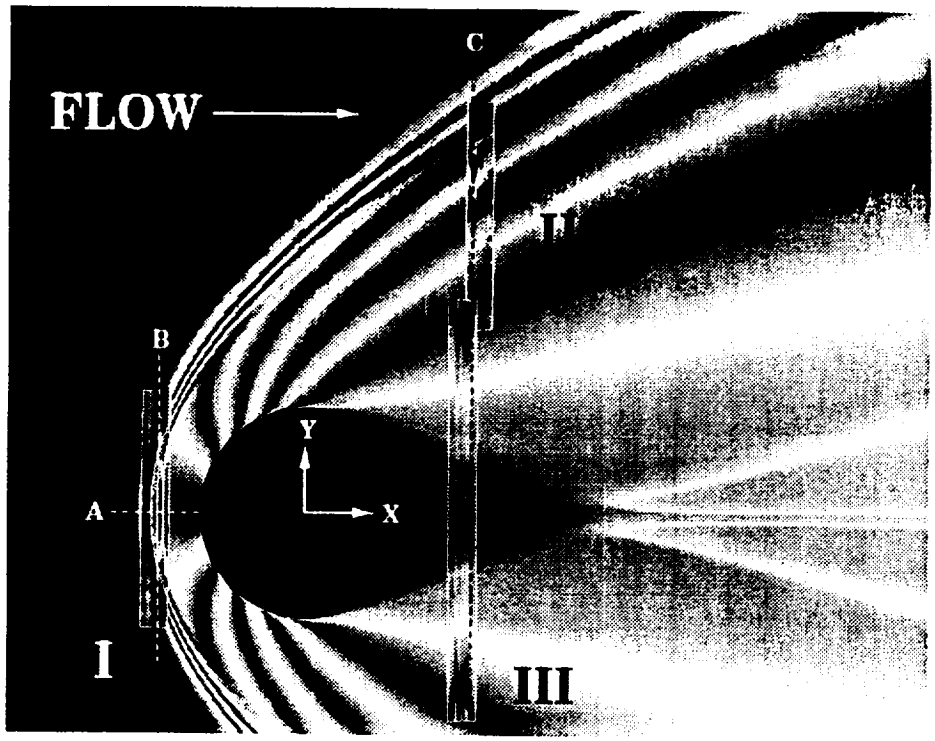

Fig. 2. Planar view of the Rayleigh and the CFD data. The Rayleigh data are shown in measurement planes designated by I, II, and III. See text for detail.

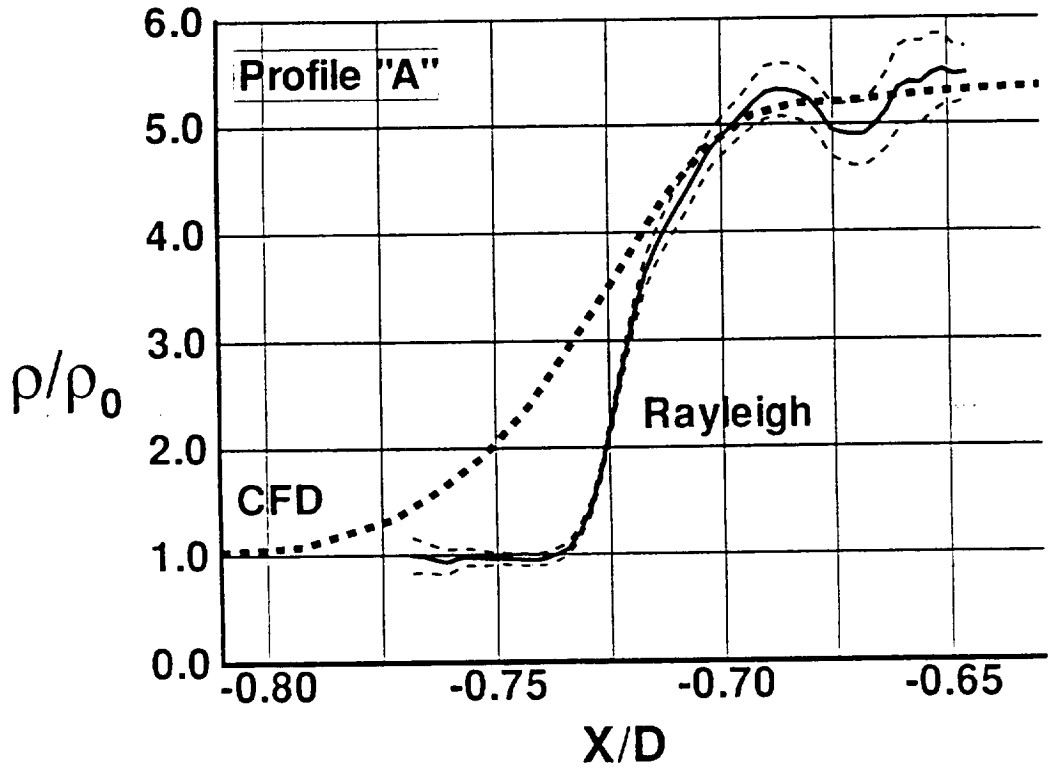

Fig. 3. Comparison between the Rayleigh and the CFD data along the profile "A" (y/D = 0) shown in Fig. 2. The dashed lines around the Rayleigh data represent the statistical uncertainties in the deduced density. See text for detail.

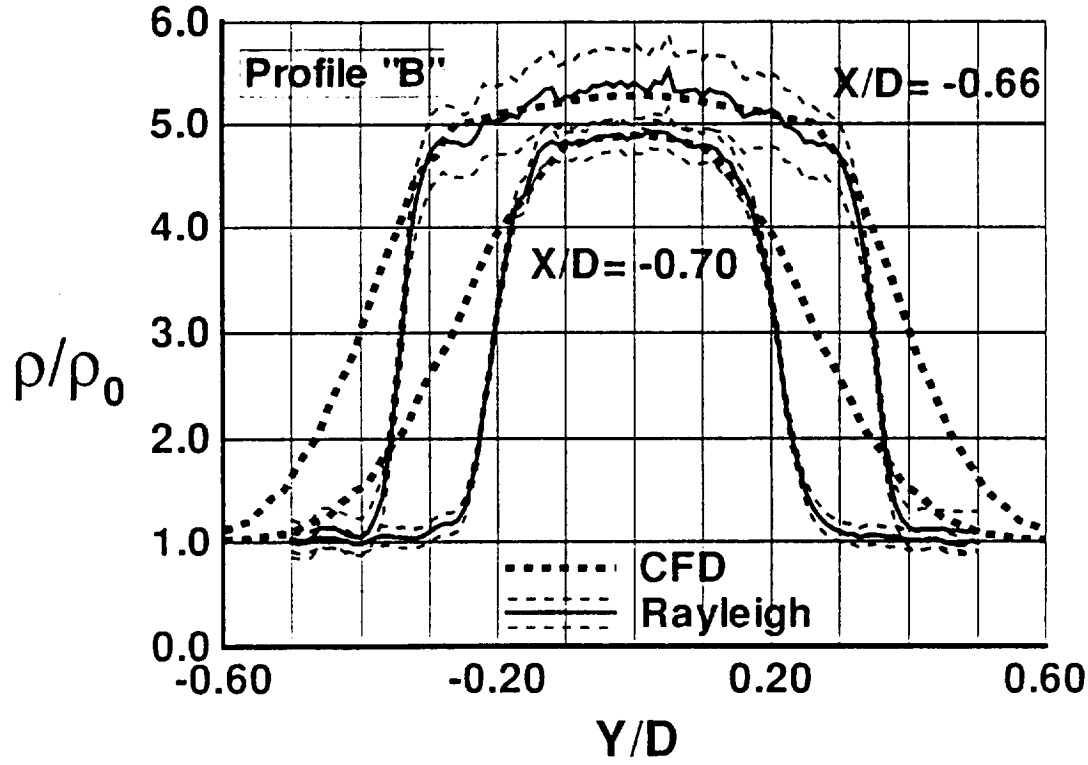

Fig. 4. Comparison between the Rayleigh and the CFD data for two x/D positions along the y-axis (profile "B" in Fig. 2). See text for detail.

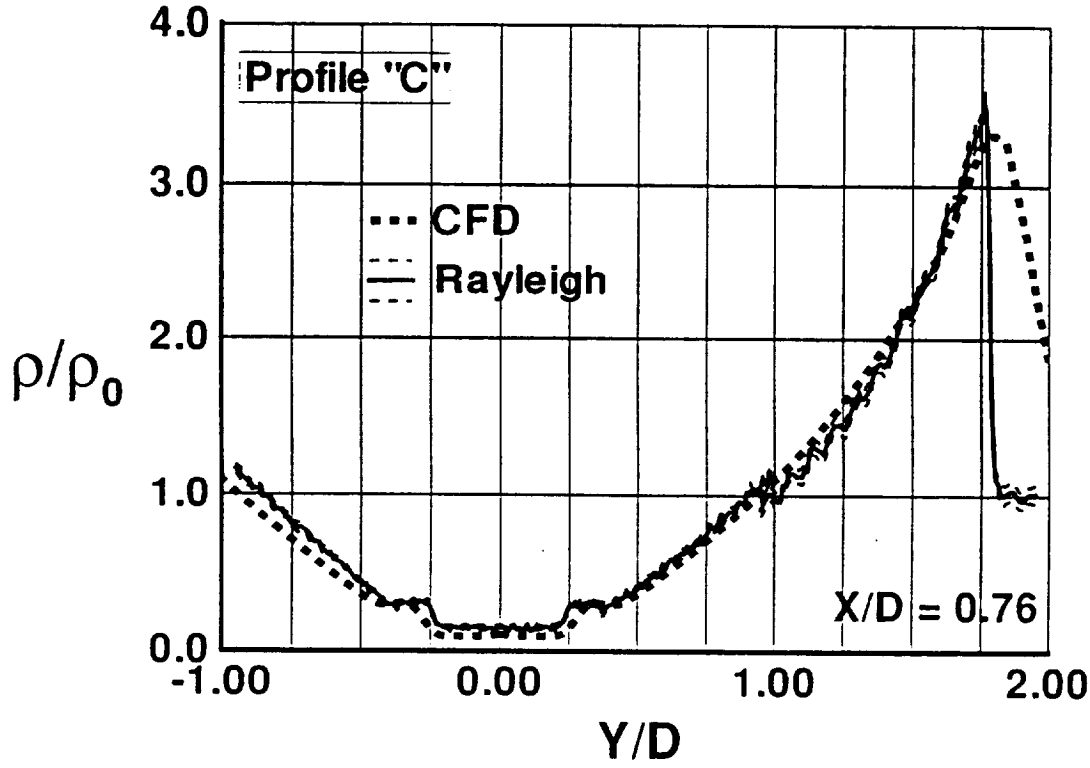

Fig. 5. Comparison between the Rayleigh and the CFD data along the profile "C" in Fig. 2. See text for detail.